Volume 219 November 2014 ISSN 0022-4596

ELSEVIER

JOURNAL OF SOLID STATE CHEMISTRY

IN THIS ISSUE:

Crystal structures and electronic properties for the over-lithiated and Li–Ag substituted phases of $Li_9V_3(P_2O_7)_3(PO_4)_2$ insertion electrode system

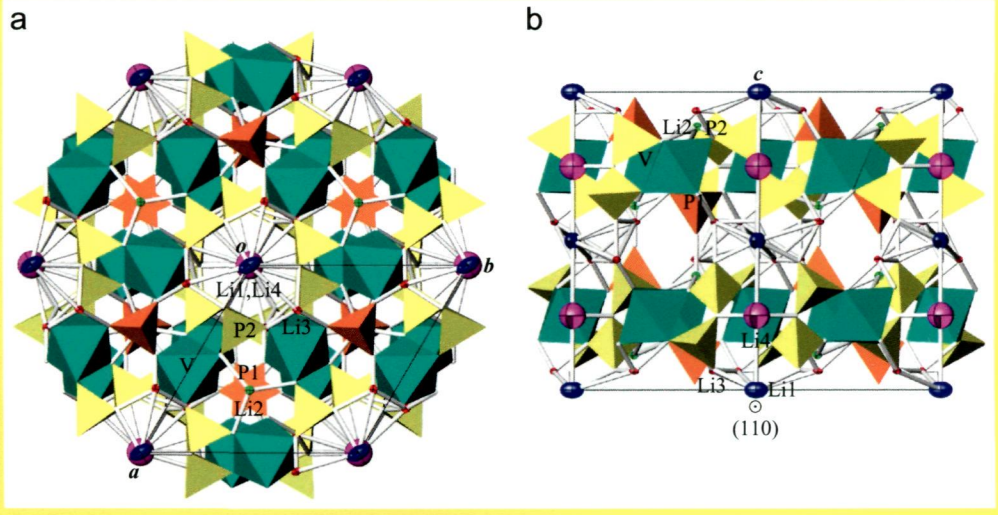

Masashige Onoda, Makoto Inagaki and Hiroaki Saito

ELSEVIER

Volume 219, November 2014

CONTENTS

JOURNAL OF SOLID STATE CHEMISTRY

www.elsevier.com/locate/jssc

Abstracted/indexed in BioEngineering Abstracts, Chemical Abstracts, Coal Abstracts, Current Contents/Physics, Chemical, & Earth Sciences, Engineering Index, Research Alert, SCISEARCH, Science Abstracts, and Science Citation Index. Also covered in the abstract and citation database SCOPUS®. Full text available on ScienceDirect®.

Regular Articles

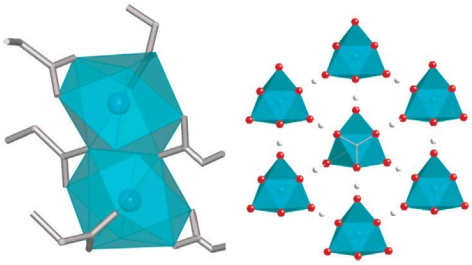

Four dysprosium (Dy) complexes with formate, propionate, butyrate and oxalate ligands have been synthesized and characterized. The Dy formato complex has a 3D pillared metal organic framework and the structure is stable up to 360 °C whilst the complexes with longer alkyl chained mono-carboxylates possess similar di-nuclear structures. The Dy oxalato complex has a 2D hexagonal (honeycomb-type) structure. Their Raman vibration modes have been investigated.

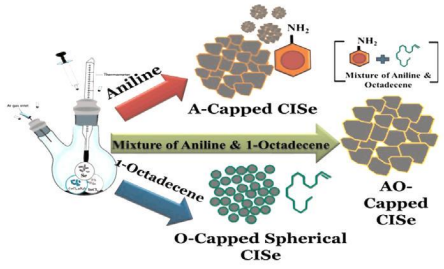

Without resorting to any post-selenization process and using the colligative properties of the mixture comprising of volatile aniline and non-volatile 1-octadecene to manoeuvre the growth conditions to promote Ostwald ripening, a single phase, monodispersive and nearly stoichiometric ternary CISe nanocrystals are formed by wet-synthesis route.

Regular Articles—Continued

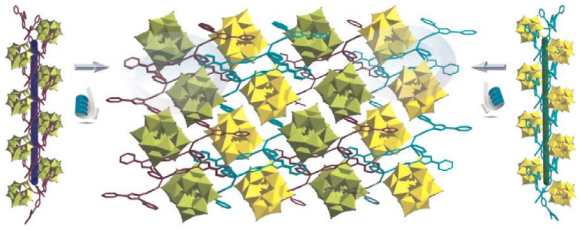

Two new compounds, $[CuH_3L_2(GeMo_{12}O_{40})]\cdot 2H_2O$ (**1**) and $[CuH_3L_2(SiMo_{12}O_{40})]\cdot 2H_2O$ (**2**) have been synthesized under hydrothermal conditions. The two compounds possess the left- and right-handed helical chains.

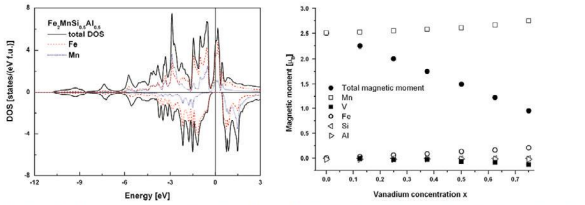

Densities of states of $Fe_2MnSi_{0.5}Al_{0.5}$ and magnetic moments of $Fe_2Mn_{1-x}V_xSi_{0.5}Al_{0.5}$.

Continued

Preparation of resveratrol-loaded nanoporous silica materials with different structures

Margarita Popova, Agnes Szegedi, Vesselina Mavrodinova, Natasa Novak Tušar, Judith Mihály, Szilvia Klébert, Niko Benbassat and Krassimira Yoncheva

page 37

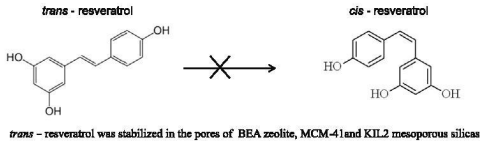

trans-Resveratrol was stabilized in the pores of BEA zeolite, MCM-41and KIL2 mesoporous silicas.

Two three-dimensional coordination polymers of lead(II) with iminodiacetate and naphthalene-dicarboxylate anions: Synthesis, characterization and luminescence behavior

Debdoot Hazari, Swapan Kumar Jana, Michel Fleck, Ennio Zangrando and Sudipta Dalai

page 43

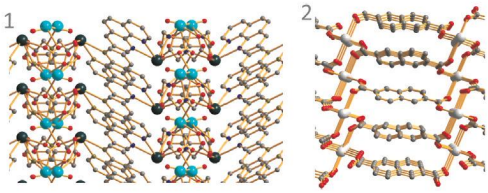

Two new topologically different 1D coordination polymers formed by Pb_4 clusters have been synthesized and characterized by x-ray analysis. The luminescence and thermal properties have been studied.

Incorporation of uranium in pyrochlore oxides and pressure-induced phase transitions

F.X. Zhang, M. Lang, C. Tracy, R.C. Ewing, D.J. Gregg and G.R. Lumpkin

page 49

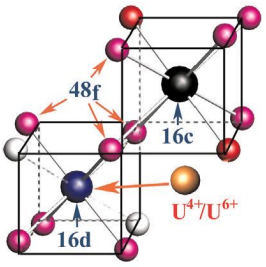

In U-bearing pyrochlore, U ions mainly occupy the 16*d* site and replace the smaller Zr^{4+}, part of the oxygen will occupy the 8*b* site, which is empty to most pyrochlores. At pressure of 22 GPa, the pyrochlore lattice is not stable and transforms to a cotunnite-type structure. The high-pressure structure is not stable and transform to a fluorite or back to the pyrochlore structure when pressure is released.

A set of alkali and alkaline-earth coordination polymers based on the ligand 2-(1*H*-benzotriazol-1-yl) acetic acid: Effects the radius of metal ions on structures and properties

Jin-Hua Wang, Gui-Mei Tang, Ting-Xiao Qin, Shi-Chen Yan, Yong-Tao Wang, Yue-Zhi Cui and Seik Weng Ng

page 55

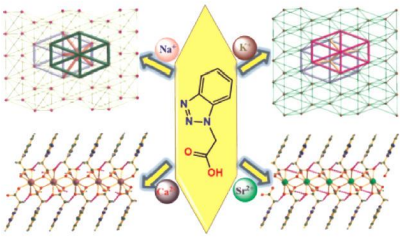

A set of alkali and alkaline-earth metal coordination polymers were hydrothermally synthesized by 2-(1*H*-benzotriazol-1-yl)acetic acid, displaying interesting topologic motifs from two-dimension to one-dimension and specific physical properties.

Dependence of catalytic properties of Al/Fe_2O_3 thermites on morphology of Fe_2O_3 particles in combustion reactions

Ningning Zhao, Cuicui He, Jianbing Liu, Hujun Gong, Ting An, Huixiang Xu, Fengqi Zhao, Rongzu Hu, Haixia Ma and Jinzhong Zhang

page 67

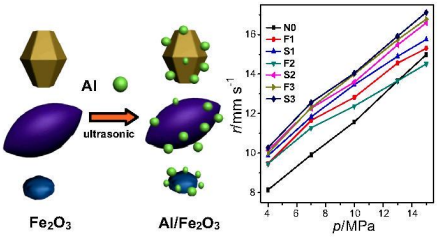

Effects of Fe_2O_3 and Al/Fe_2O_3 have been compared for the first time by analyzing combustion properties of formulations containing them, suggesting their potential application in AP/HTPB composite propellant systems.

Ba_3GeS_5 and Ba_3InS_4Cl: Interesting size effects originated from the tetrahedral anions

Ming-Yan Pan, Sheng-Qing Xia, Xiao-Cun Liu and Xu-Tang Tao

page 74

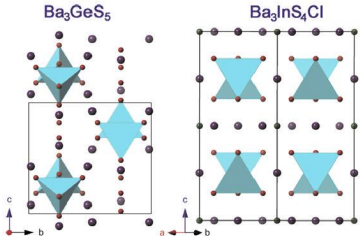

The polyhedral structure view for Ba_3GeS_5 and Ba_3InS_4Cl in which Ba, S and Cl atoms are plotted in purple, red and green spheres.

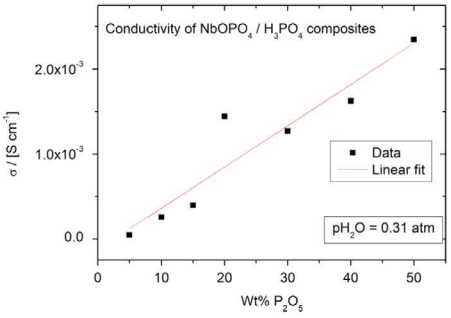

Conductivity of $NbOPO_4/H_3PO_4$ composites as a function of equivalent P_2O_5 content. The conductivity is insignificant for pure $NbOPO_4$.

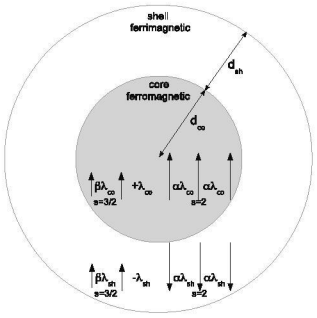

Core–shell model: The core has a ferromagnetic character, while the shell is ferrimagnetic. Each one has two sub-lattices (Mn^{3+} and Mn^{4+}) that interact through a mean-field (see Eq. (6)). Interactions strength and signals are also represented in this figure. In this figure the arrows (or vectors) represent the magnetic moment of ions Mn^{3+} (s=2) and Mn^{4+} (s=3/2). $\beta\lambda$'s describe the ferromagnetic interaction between Mn^{4+} ions into the core ($\beta\lambda_{co}$) and into the shell ($\beta\lambda_{sh}$), while $\alpha\lambda$'s represent ferromagnetic interaction between Mn^{3+} ions into the core ($\alpha\lambda_{co}$) and into the shell ($\alpha\lambda_{sh}$). The $-\lambda_{sh}$ and $+\lambda_{co}$co are associated to the mean field parameter of interaction between Mn^{3+} and Mn^{4+} sub-lattices in the shell (ferrimagnetic, negative sign) and core (ferromagnetic, positive sign), respectively.

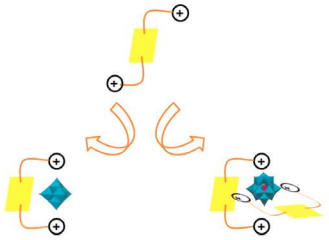

Hybrid molecular materials with charge-transfer characters formed by a positively charged donor L and acceptors of the Lindqvist-type and Keggin-type POMs have lamellar and cubic structures in their solid state.

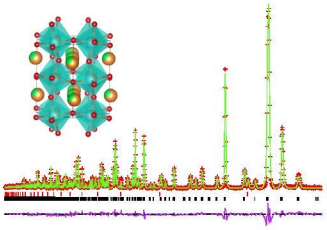

Atomistic model of $Sr_{0.3}Nd_{0.7}Mg_{0.35}Ti_{0.65}O_3$ and Rietveld refinement of neutron diffraction data.

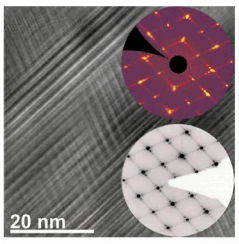

High-resolution transmission electron micrograph, SAED pattern and reciprocal lattice section of X-ray single crystal data of $Ge_{3.25}Sn_{1.1}Sb_{1.1}Te_6$ with an 11*P*-type superstructure of the rocksalt type.

Continued

Controllable hydrothermal synthesis of rutile TiO_2 hollow nanorod arrays on $TiCl_4$ pretreated Ti foil for DSSC application

Min Xi, Yulan Zhang, Lizhen Long and Xinjun Li

page 118

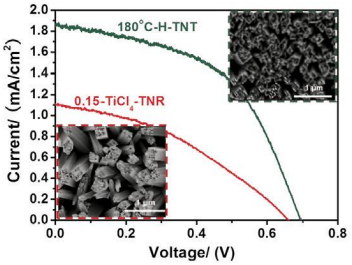

Rutile hollow TiO_2 nanorod array photoanode obtained from original TiO_2 nanorod array photoanode by hydrothermal etching demonstrates enhanced photoelectric efficiency of DSSC.

Structural, vibrational and luminescence properties of the $(1-x)CaWO_4-xCdWO_4$ system

A. Taoufyq, F. Guinneton, J-C. Valmalette, M. Arab, A. Benlhachemi, B. Bakiz, S. Villain, A. Lyoussi, G. Nolibe and J-R. Gavarri

page 127

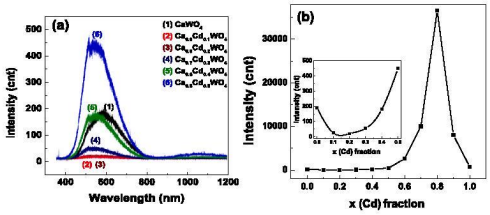

Luminescence on UV excitation (364.5 nm) of $(1-x)CaWO_{4-x}CdWO_4$ system, elaborated from coprecipitation technique at 1000 °C, with $0<x<1$. (a) Experimental emission bands of the $Ca_{1-x}Cd_xWO_4$ polycrystalline phases with $0\leq x\leq 0.5$. (b) Maximum of luminescence intensity for the composition $x=0.8$.

The interaction between cations and anionic groups inducing SHG enhancement in a series of apatite-like crystals: A first-principles study

Qun Jing, Xiaoyu Dong, Zhihua Yang, Shilie Pan, Bingbing Zhang, Xuchu Huang and Mingwei Chen

page 138

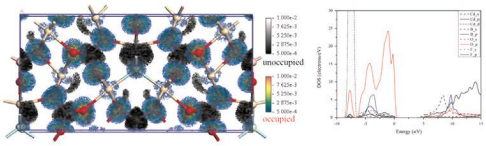

Combined with the first-principles method, SHG-density method and real-space atom-cutting method, the enhancement of SHG response are attributed to the interaction between cadmium and BO_3 groups.

Thermal expansion and phase transitions of α-AlF_3

Cody R. Morelock, Justin C. Hancock and Angus P. Wilkinson

page 143

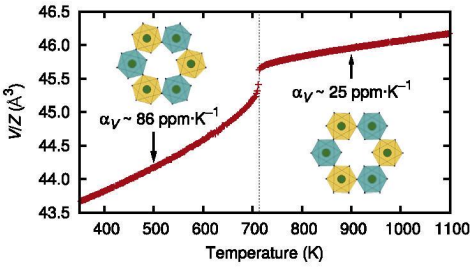

α-AlF_3 has a rhombohedrally distorted ReO_3-type structure at ambient conditions and displays strongly positive volume thermal expansion that is highly anisotropic; the material becomes cubic on heating above ~713 K and continues to show positive thermal expansion.

Structural and magnetic characterisation of the novel spin frustrated double perovskite Sr_2ScMoO_6

Thomas K. Wallace and Abbie C. Mclaughlin

page 148

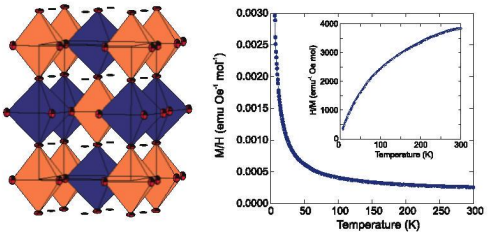

A novel double perovskite Sr_2ScMoO_6 has been synthesised which has corner sharing MoO_6 and ScO_6 octahedra. The Sr^{2+} cations reside in the cavities and exhibit anisotropic thermal motion. There is no evidence of magnetic order down to 6 K.

High magnetic field induced spin flip/flop behavior and magnetic phase diagram of $CuFe_{1-x}Ga_xO_2$

L.R. Shi, Z.C. Xia, Z. Jin, M. Wei, J.W. Huang, B.R. Chen, L.X. Xiao, H.K. Zuo and Z.W. Ouyang

page 152

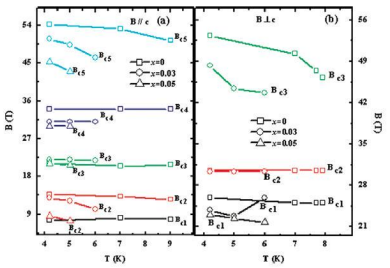

Temperature dependence of the critical fields for $CuFe_{1-x}Ga_xO_2$ (x=0, 0.03, 0.05). (a) and (b) The magnetic field's parallel and perpendicular cases respectively. In which, the square, circle and triangular represent x=0, 0.03 and 0.05 respectively.

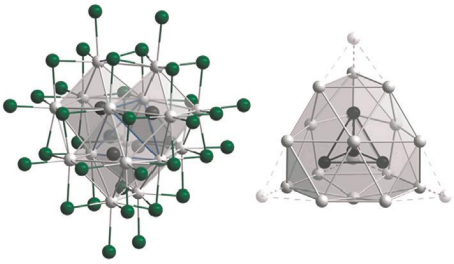

Rare earth-metal cluster complexes with endohedral transition metal atoms $\{TR_6\}$ may connect via common edges or faces to form dimers, trimers, tetramers and pentamers of which the tetramers are the most prolific. Packing effects and electron counts play an important role.

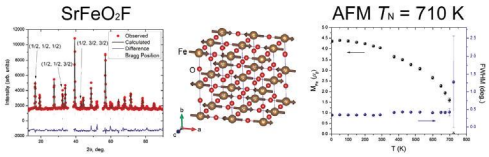

Variable temperature powder neutron diffraction was employed to follow the evolution of the long range antiferromagnetic state in $SrFeO_2F$.

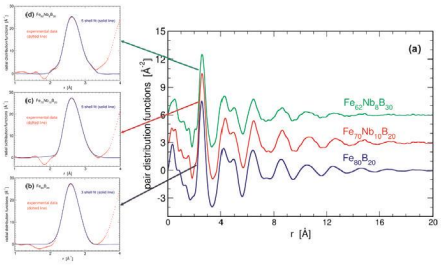

Pair distribution functions (a) and best-fit model and experimental radial distribution functions for $Fe_{80}B_{20}$ (b), $Fe_{70}Nb_{10}B_{20}$ (c) and $Fe_{62}Nb_8B_{30}$ (d) metallic glasses.

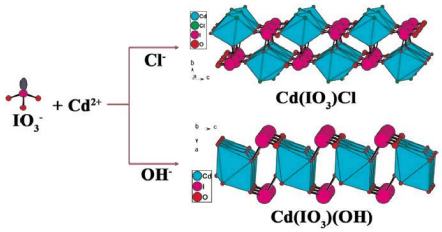

Two new layered cadmium iodates $Cd(IO_3)X$ (X=Cl, OH) are reported. $Cd(IO_3)Cl$ features a unique double layered structure whereas $Cd(IO_3)(OH)$ displays an ordinary layered structure.

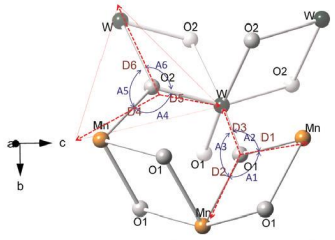

Despite of substitution of smaller In^{3+} for larger Mn^{2+}, the In-rich solid solution $Mn_{0.71(2)}In_{0.19(1)}\square_{0.10}WO_4$ undergoes a volume expansion of 0.4% with respect to $MnWO_4$. This could be explained by a local space expansion of 0.13% around bridging oxygen at O2 sites, as illustrated by dashed lines for clarity.

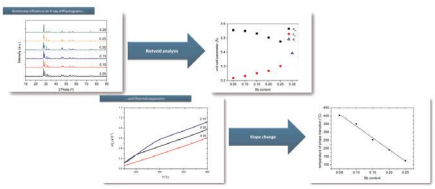

Substitution of niobium by other pentavalent elements in $LaNbO_4$ leads to change in phase transition temperature. In case of Sb substituent a shift of phase transition into the lower temperature region is observed. $LaNb_{0.7}Sb_{0.3}O_4$ substitution allows to achieve material with tetragonal crystal structure at room temperature and no phase transition up to 1000 °C.

Continued

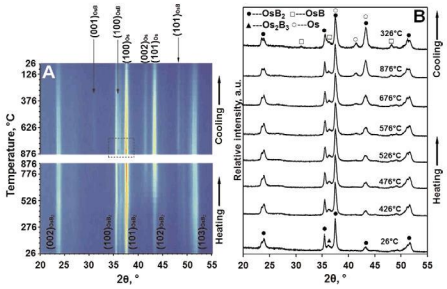

The *in situ* high temperature XRD contour plot (A) and XRD patterns (B) of *h*-OsB_2 upon heating and cooling under an argon atmosphere.

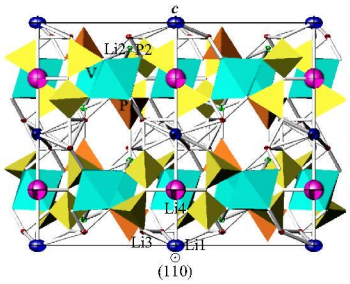

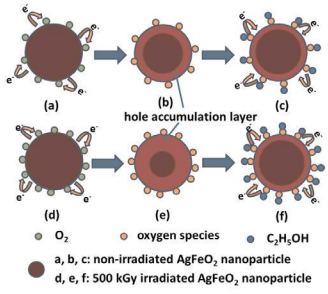

Gamma ray irradiation improved the performance of gas sensor based on the $AgFeO_2$ nanoparticles including sensitivity and optimum operating temperature, which might be ascribed to the generation of defects.

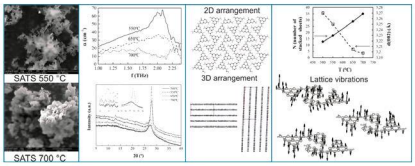

2D lattice mode vibrations and structural changes correlated with the so called "2D to 3D transition".

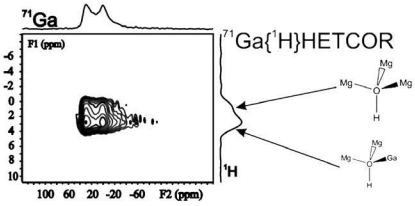

Two types of hydroxides groups are observed in magnesium gallium layered double hydroxides revealing an ordering of Ga in the cation layer.

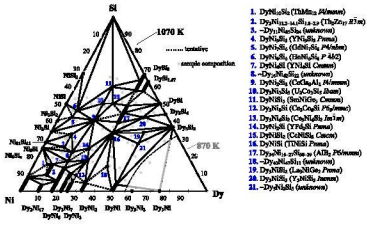

The Dy–Ni–Si system has been investigated at 1070 K by X-ray and microprobe analysis. The system contains the 12 known compounds $DyNi_{10}Si_2$, $DyNi_5Si_3$, $DyNi_6Si_6$, $DyNi_4Si$, $DyNi_2Si_2$, $Dy_2Ni_3Si_5$, $DyNiSi_3$, $Dy_3Ni_6Si_2$, $DyNiSi_2$, $DyNiSi$, Dy_3NiSi_3, Dy_3NiSi_2, and the new compounds $Dy_{34}Ni_{16-27}Si_{50-39}$, $Dy_2Ni_{15.2-14.1}Si_{1.8-2.9}$, ~$Dy_{11}Ni_{65}Si_{24}$, ~$Dy_{16}Ni_{62}Si_{22}$, $DyNi_7Si_6$, Dy_3Ni_8Si, $DyNi_2Si$, ~$Dy_{40}Ni_{47}Si_{13}$ and ~$Dy_5Ni_2Si_3$. Quasi–binary solid solutions were detected for Dy_2Ni_{17}, $DyNi_5$, $DyNi_7$, $DyNi_3$, $DyNi_2$, $DyNi$, $DySi_2$ and $DySi_{1.67}$. The crystal structures and magnetic properties of new phases RNi_7Si_6 ($GdNi_7Si_6$-type), R_3Ni_8Si (Ce_3Co_8Si-type), RNi_2Si (YPd_2Si-type) and $R_3Ni_{12}Si_4$ ($Gd_3Ru_4Al_{12}$-type), with R=Y, Gd–Tm, are also reported.

Syntheses, structures, molecular and cationic recognitions and catalytic properties of two lanthanide coordination polymers based on a flexible tricarboxylate

Yu Zhu, Yan-Mei Wang, Ji Xu, Pan Liu, H.A.B.M.D. Weththasinha, Yun-Long Wu, Xiao-Qing Lu and Ji-Min Xie

page 259

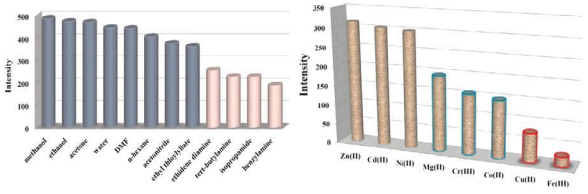

We have synthesized two isostructural 3D compounds based on H_3TTTA. They are chemical sensor of amine solvents and cations. They have higher yields and TOFs to catalyze cyanosilylation reactions.

Intergrowth structure of α-phase in β-type $TmAlB_4$ compound studied by high-angle annular detector dark-field scanning transmission electron microscopy

Kunio Yubuta, Takao Mori, Andreas Leithe-Jasper, Horst Borrmann, Yuri Grin, Shigeru Okada and Toetsu Shishido

page 274

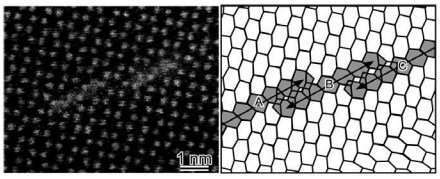

Nanostructure of a $ThMoB_4$-type (β-type) $TmAlB_4$ compound, in which $YCrB_4$-type (α-type) domains are locally intergrown, is studied by high-angle annular detector dark-field scanning transmission electron microscopy (HAADF-STEM). *Z*-contrast images by HAADF-STEM directly represent arrangements of Tm atoms located at centers of heptagonal atomic columns of B atoms as bright dots, and give us detailed information of the characteristic intergrowth structure of type domains in the matrix of the β-type phase.

Acidic 1,3-propanediaminetetraacetato lanthanides with luminescent and catalytic ester hydrolysis properties

Mao-Long Chen, Yan-Ru Shi, Yu-Chen Yang and Zhao-Hui Zhou

page 265

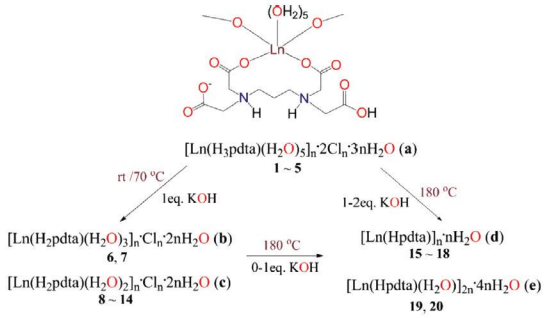

A series of water-soluble acidic 1,3-propanediaminetetraacetato lanthanides $[Ln(1,3\text{-}H_3pdta)(H_2O)_5]n\cdot 2Cl_n\cdot 3nH_2O$ have been converted to their 2D and 3D lanthanides, which are active for the catalytic conversion of ester hydrolysis.

Rapid Communications

First single crystal growth and structural analysis of superconducting layered bismuth oxyselenide; $La(O,F)BiSe_2$

Masashi Tanaka, Masanori Nagao, Yoshitaka Matsushita, Masaya Fujioka, Saleem J. Denholme, Takahide Yamaguchi, Hiroyuki Takeya and Yoshihiko Takano

page 168

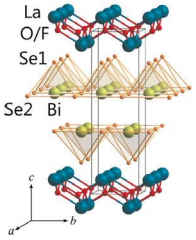

Single crystal $La(O,F)BiSe_2$ has been prepared by a CsCl flux method. The structural analysis implies that $La(O,F)BiSe_2$ is a potential superconductor having a higher T_c under high pressure.